Lifetime of an excited atom in a metal cavity

K. Ohtaka* and A. A. Lucas
Département de Physique, Facultés Universitaires Notre-Dame de la Paix, Namur, B-5000 Namur, Belgium
(Received 8 May 1978)

Several broadening mechanisms for an optical absorption line of a gas atom or molecule trapped in a spherical cavity in a metallic host are examined. Among these, the linewidth due to the coupling of the atom to damped surface polaritons of the metal cavity is analyzed in detail, and its dependence on cavity radius and on atom position is obtained. One finds that the surface-polariton coupling effect is important only for bubbles of atomic sizes (a few vacancy clusters), or for resonant cases where the atomic frequency coincides with one of the surface-plasmon frequencies. Numerical application is made to the broadening of the resonance line of helium trapped in an aluminum matrix. For this system the polariton coupling appears to be negligible as compared to the so-called resonance broadening in the gas under the pressures which are presumed to prevail in bubbles produced by He implantation. The optical absorption of a random distribution of small He-gas bubbles in Al is also computed by means of an effective-medium theory. One finds that the absorption linewidth and position should give a good measure of the average He density in the bubbles.

I. INTRODUCTION

The irradiation of metals with energetic He ions, α particles, or He-generating radiations such as neutrons, creates extended damage in the form of He bubbles[1,2] trapped in the metal matrix. The bubble size may range from a few angstroms to several micrometers, depending on radiation dose, specimen temperature, and other irradiation conditions. At high doses, blisters appear at the surface of the target as a result of large bubbles developing and eventually bursting in the surface region.

The formation of such internal cavities causes bulk swelling, surface flaking, and adverse consequences for the mechanical properties of structural materials in the core of nuclear fission and fusion reactors. Consequently, a great deal of efforts has been devoted to the study and control of this phenomenon by a variety of experimental as well as theoretical methods.[3-6]

One important parameter for bubble nucleation and growth is the He pressure inside the cavity.[7,8] Depending on the He injection dose and bubble size, the pressure is presumed to vary from zero in so-called voids to tens of kilobars, exceeding the yield strength of the surrounding metal, in overpressurized bubbles.

Although several studies of bubble formation in He-bombarded metals assume that the He gas pressure in small cavities is in equilibrium with the surface-tension pressure,[8] one does not really have a direct experimental mean to verify this hypothesis or to measure the actual pressure in over- or underpressured bubbles.

Perhaps one way of having access to this information would consist in measuring a spectroscopic property of trapped He which would exhibit sufficient pressure sensitivity. One such property might be the position, the width, or the detailed line shape of an atomic absorption line for uv radiation such as the strong resonance line of the principal series ($1\,^1S_0 \rightarrow n\,^1P_1$, $n=2$) of He at 584.3 Å or 21.2 eV.[9,10] However the usefulness of this spectroscopic method will depend on our ability to evaluate the numerous mechanisms influencing the line shape of an atom trapped in a bubble as much as on the experimental capability to discriminate the atomic absorption from the metal background.

The purpose of the present paper is (i) to study a number of causes of line broadening for an individual gas atom in a spherical metal cavity and (ii) to compute the bubble absorption line shape in the framework of a simple macroscopic theory.

One particular mode of line broadening which may be expected to be important for small bubble radii is the long-range interaction between the atom and the surrounding metal matrix. A satisfactory description of the metal in this context is by means of a complex dielectric function $\epsilon(\omega)$ embodying the only metal excitation which responds to the high-frequency atomic excitation external to the metal surface, namely, the plasmon oscillations.[11] The real part of ϵ causes line broadening by inhomogeneously shifting the atomic levels as a result of Van der Waals interactions whereas the imaginary part of ϵ enhances the linewidth by providing the possibility for the atomic excitation to be carried away by the substrate.

Related problems have been studied by Morawitz and Philpott,[12] Chance, Prock, and Silbey,[13] and Agarwal and Vollmer[14] who have shown that an excited molecule near a flat metal surface may de-

cay faster than in free space through resonant excitation of surface polaritons. In the present work we shall extend the theory to the spherical geometry of a cavity and also the plasmon damping will be included and shown to be important.

After discussing the absorption line shape from the atomic point of view, we then turn to a macroscopic description of the porous metal in which the gas bubbles are treated as spherical regions of homogeneous dielectric function $\epsilon_g(\omega)$, surrounded by the continuous metallic substrate of dielectric function $\epsilon(\omega)$. When the wavelengths of interest are much larger than the average bubble radius, the optical properties of the system may be described in terms of an average dielectric function $\bar{\epsilon}(\omega, f)$ depending only on the volume fraction f occupied by the bubbles, as shown in recent works by Barker,[15] Genzel and Martin,[16] and Grandqvist and Hunderi[17] in different contexts. This simple approach readily provides the absorption line position and width. If the wavelengths are of order or smaller than the bubble dimension, then the full Mie theory[17,18] of light scattering by spheres should be applied. This will not be attempted here.

Throughout the paper, numerical application will be made for the system of He bubbles in aluminum. The reason for choosing this combination is that aluminum, besides being a metal of nuclear technological interest, is one of the most transparent to uv light in the 20-eV energy range and hence offers the best conditions for He detection by selective optical absorption.[19]

In Sec. II we shall briefly review the broadening mechanisms of the gas phase such as listed in Table I. In Sec. III the effects of the metal matrix listed in this table will be analyzed. Section IV contains the average-medium dielectric approach and Sec. V draws the conclusions of the present work.

TABLE I. Two classes of line-broadening effects for an optical excitation line of an atom in a bubble.

Gas-phase effects	Substrate effects
1. Radiation damping	1. Wall collision
2. Doppler effect	2. Physisorption
3. Van der Waals broadening	3. Surface-polariton effects
a. Ground state	a. Modified radiation damping
b. Excited state (resonance broadening)	b. Inhomogeneous shift
	c. Plasmon decay
Others	

II. BROADENING EFFECTS IN THE GAS PHASE

A. Radiation damping

For future reference we recall here the formula for the radiation linewidth[20,21] in empty space [full width at half maximum (FWHM)] of a resonant transition originating from level 1 and ending in the ground level 0 (no other one-photon transition is allowed for the resonance level of an isolated He atom)

$$\gamma_0 = (2e^2\omega_0^2/mc^3) f_{10} . \tag{1}$$

where ω_0 is the (angular) frequency of the transition and f_{10} its oscillator strength. The accurate value of f_{10} is known[22,23] for the $2\,^1P_1 \rightarrow 1\,^1S_0$ transition in He but we shall be satisfied here to use the approximate value $f_{10} \simeq \frac{1}{3}$ which makes formula (1) coincide with the Lorentzian width of a classical damped oscillator

$$\gamma_0 = 2e^2\omega_0^2/3mc^3 . \tag{2}$$

This gives a relative width $\gamma_0/\omega_0 \simeq 1.5\times 10^{-7}$ for the 584.3-Å resonant line of He. The radiative width of this resonant line of He in a metal cavity will be discussed in Sec. III.

B. Doppler width

If one could treat the He gas in high-pressure bubbles as a perfect gas, the relative Doppler width would be[20,21]

$$\frac{\gamma_D}{\omega_0} = 2(2\ln 2)^{1/2}\left(\frac{RT}{Mc^2}\right)^{1/2} \simeq \frac{\bar{v}}{c} , \tag{3}$$

where T is the temperature, M the molecular weight, and $\bar{v}$ some average velocity. At room temperature this gives $\gamma_D/\omega_0 \simeq 10^{-5}$, i.e., much larger than the natural width γ_D seen above. However we shall see that the major broadening mechanisms are much more important than this. Hence there is no need to use the Van der Waals or other equations of states[24] to obtain a better estimate of the negligible Doppler width.

C. Van der Waals broadening

It is customary to distinguish between two kinds of Van der Waals broadening for a pure gas[20]: (a) the inhomogeneous broadening of the line due to the statistical shift of the ground-state level of interacting atoms and (b) the inhomogeneous broadening of the excited level resulting from resonant transfer of energy from the excited atom to the neighboring unexcited ones. The latter effect is the so-called resonance broadening and constitutes the dominant source of line broadening in pure gases at most temperatures and pressures.[20,21,25]

For a model, which we shall be using throughout the paper, in which the He atom is represented by

a single isotropic oscillator, it is easy to describe the basic reason of Van der Waals broadening: two such isotropic oscillators separated by a distance d and interacting through a nonretarded dipole field have six modes of vibration with frequencies given by

$$\omega_a^{(\pm)} = \omega_0\left(1 \pm 2\,\frac{\alpha_0}{d^3}\right)^{1/2} \quad (m=0) \tag{4}$$

for the two nondegenerate axial modes (magnetic quantum number $m=0$) of even (+) or odd (−) parity with respect to inversion symmetry and

$$\omega_t^{(\pm)} = \omega_0\left(1 \mp \frac{\alpha_0}{d^3}\right)^{1/2} \quad (m=\pm 1) \tag{5}$$

for the two degenerate transverse modes ($m=\pm 1$). In these expressions

$$\alpha_0 = (e^2/m\omega_0^2) f_{10} \simeq 0.15\ \text{Å}^3 \tag{6}$$

is a measure of the He ground-state static polarizability. The ground-state energy of the pair is, for all molecular orientations,

$$E_0 = 3\hbar\omega_0(1 - \alpha_0^2/4d^6)\,. \tag{7}$$

Equation (7) is the dipole analog of the origin of the broadening (a), which leads to an inhomogeneous blue shift of the excitation energy. Expressions (4) and (5) of the level splittings, on the other hand, result in a symmetric broadening (taking into account the degree of degeneracy and the dipole selection rule of the optical excitation) and express the classical origin of the broadening (b).

1. *Ground-state broadening*

The line shape which results from this broadening (neglecting the resonance effect discussed below) is derived by treating statistically the second term of Eq. (7). Using the additivity of the d^{-6} shift with respect to possible atom pairs, Margenau[20] obtained the highly asymmetric line shape:

$$I(\omega) = \begin{cases} 0 & \text{for } \omega < \omega_0\,, \\ (\omega-\omega_0)^{-3/2} e^{-\pi\lambda^2/(\omega-\omega_0)} & \text{for } \omega > \omega_0\,, \end{cases} \tag{8}$$

where

$$\lambda = \tfrac{2}{3}\pi\sqrt{b}\,n$$

in which n is the He number density and b is the constant which appears in the ground-state attraction energy of a pair of neutral atoms written as $-\hbar b/d^6$. For the He model of Eq. (7) this constant is of order[26] $b = \frac{3}{4}\omega_0\alpha_0^2 \simeq 5\times 10^{-34}$ cm^6 sec^{-1}. The FWHM of this line is given by

$$\frac{\gamma_v^g}{\omega_0} = 1.85\pi\,\frac{\lambda^2}{\omega_0} \simeq 25\,\frac{bn^2}{\omega_0}\,. \tag{9}$$

Even at liquid-He densities $n \sim 5\times 10^{22}$ cm^{-3}, this does not exceed $\gamma_v^g/\omega_0 \simeq 10^{-3}$.

2. *Resonance broadening*

For a randomly distributed N-atom system a correct statistical treatment of the level splitting Eqs. (4) and (5) is difficult, because the level splitting is not additive in contrast to Sec. II C 1 (consider, for example, the dispersion relation of the Frenkel exciton in the translationally invariant system). The line shape and width are calculated concentrating on an isolated pair of atoms. Several authors arrived at the line shape[20,21]

$$I(\omega) = \frac{\alpha_0 n}{(\omega-\omega_0)^2} \quad \text{for } |\omega-\omega_0| \gg \omega_0\,, \tag{10}$$

with the FWHM

$$\gamma_v^r/\omega_0 = C\alpha_0 n \simeq 10\alpha_0 n\,, \tag{11}$$

where C is a dimensionless constant of order 10 whose precise value depends on which type of theory is used.[21] Using again a liquid density to evaluate the expected maximum broadening one finds $\gamma_v^r/\omega_0 \simeq 0.05$, i.e., an order of magnitude larger than the ground-state Van der Waals broadening.

We conclude that since the resonance width is proportional to density n, in contrast to the ground-state broadening [Eq. (9)], the former should be the dominant cause of line broadening within the gas phase over the complete range of bubble pressures.

III. SUBSTRATE EFFECTS ON LINEWIDTH

A. Wall collisions

For the smallest bubbles, the mean free path of the atom for collisions becomes limited by the bubble size. The frequency of collisions with the bubble wall, to which transfer of the atomic excitation may occur, is of order $\bar{v}/a$, where a is the radius of the bubble. This gives a wall-collision broadening

$$\gamma_{WC}/\omega_0 \simeq \bar{v}/a\omega_0\,. \tag{12}$$

For a bubble made of a few atomic vacancies in Al, one may estimate $a \gtrsim 4$ Å and $\gamma_{WC}/\omega_0 \leq 10^{-4}$. For larger bubbles, the wall-collision frequency becomes negligible as compared to other decay rates of the problem.

B. Physisorption

It has been suggested[8] that under the high pressure prevailing in small bubbles, the wall may be covered by some layer of condensed He. The electronic states of such adsorbed atoms are broadened to bands. Then there must be a corresponding broadening of the optical-absorption line, the upper level of which is broad resonance in the metal

conduction-band states.[27] Unfortunately, to our knowledge, calculations of such a band structure are not yet available for He on metal.

The ratio $3n_s/an_v$ of the number of physisorbed atoms to that of gas atoms (n_s and n_v are surface and volume densities, respectively) may be evaluated from the Gibbs adsorption equation, but should rapidly drop to negligible values for bubble radii exceeding, say, 10 Å. Hence, beyond the bubble nulceation stage, the effect of physisorption, if any, is expected to become weak for two reasons: desorption due to pressure drop and decrease of relative population of surface He versus gas He.

C. Surface-plasmon effects

We now turn to one major objective of the present work: the calculation of the effect on linewidth of the coupling of the atomic excitation to the surrounding metal though the mediation of surface plasmons. The geometry which we consider is presented in Fig. 1: the origin is at the center of the cavity with the radius a and the atom, on the z axis, is at the distance r_0 from the center and z from the cavity wall.

As in Morawitz and Philpott's work,[12] the He atom will be treated as a point dipole of eigenfrequency ω_0, charge e, and mass m. The metal substrate will be characterized by a dielectric function $\epsilon(\omega)$ appropriate to its response to the high-frequency external perturbation ($\hbar\omega_0 = 21.2$ eV). In a free-electron-like material such as Al, one uses

$$\epsilon(\omega) = 1 - \omega_p^2/(\omega^2 + i\omega g), \tag{13}$$

where $\omega_p = (4\pi n_e e^2/m)^{1/2}$ is the so-called bulk-plasma frequency and g is some damping constant

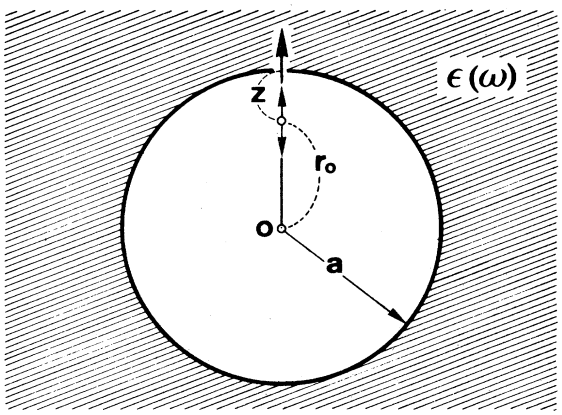

FIG. 1. Geometry for the atom-in-a-bubble problem. The bubble is assumed spherical (radius a) and the atom sits at distance r_0 from the center or $z = a - r_0$ from the wall. The metal substrate is characterized by a complex dielectric function $\epsilon(\omega)$.

which will be assumed to be frequency independent. As is seen from the work of Hagemann *et al.*,[28] formula (13) is a good approximation for Al and for $\hbar\omega$ around the He excitation energy.

The coupling with the substrate occurs because the fluctuating dipole field of the atom drives the surface-plasmon oscillations of the cavity. This coupling, which strongly depends on the atom-surface distance, causes the atomic frequency to shift [through $\mathrm{Re}\epsilon(\omega)$] and to broaden [through $\mathrm{Im}\epsilon(\omega)$]. Both effects will ultimately result in broadening of the He-gas resonance line when we take account of the statistical distribution of atom-surface distances in the gas bubble. If we write the position-dependent oscillator frequency and its energy-damping constant as $\omega(r_0)$ and $\gamma(r_0)$, the overall line shape for incoherent absorption in a spherical bubble should be proportional to

$$I(\omega) = \int_0^{a-z_0} r_0^2 n(r_0)\,\mathrm{Im}\frac{1}{\omega - \omega(r_0) - i[\frac{1}{2}\gamma(r_0)]}dr_0\,, \tag{14}$$

where z_0 is the minimum atom-surface distance and $n(r_0)$ the local gas density. Although the line shift and line broadening give nonadditive contributions to the final linewidth, we first evaluate the two effects separately in what follows.

To compare the surface-polariton effects of the cavity geometry with those of the flat-metal case, we formulate the problem taking into account the retardation effect. Effects associated with the plasmon excitation discussed above will be obtained by considering the nonretardation regime of the full result.

1. Formulation

To simplify somewhat the calculation, we shall restrict ourselves to radial dipole oscillations. The tangential dipole modes can also be treated analytically but one finds nothing drastically new but some anisotropy of the decay rate and level shift, whereas the functional dependence on r_0 and a of the quantities $\omega(r_0)$ and $\gamma(r_0)$ of Eq. (14) remains the same for both dipole orientations.

The classical calculations proceed along the lines indicated by Sommerfeld[29] in his treatment of a vertical radio antenna on the spherical earth surface (here we have a hollow-earth surface).

The time dependence of the $\vec{E}$ and $\vec{H}$ fields are assumed to be of the form $\vec{E}(\vec{r})e^{i\omega t}$, etc., and one must solve Maxwell's equations plus boundary conditions at the cavity surface. The symmetry of the problem allows us to use the spherical coordinates (r, θ, φ) and to restrict the field components to the three φ-independent variables E_r, E_θ, and H_φ.

With the introduction of a scalar potential $u(r, \theta)$ by the definition

$$H_\varphi(\vec{r}) = i\omega\epsilon(\vec{r})\frac{\partial u}{\partial \theta}, \tag{15}$$

the other field components are expressed

$$E_r(\vec{r}) = -\frac{1}{r\sin\theta}\frac{\partial}{\partial\theta}\left(\sin\theta\frac{\partial u}{\partial\theta}\right), \tag{16}$$

$$E_\theta(\vec{r}) = \frac{1}{r}\frac{\partial^2}{\partial r\partial\theta}(ru). \tag{17}$$

The Maxwell equations then reduce to the scalar Helmholtz equation

$$\Delta u + \epsilon(\vec{r})k_0^2 u = 0. \tag{18}$$

In Eqs. (15) and (18) we employed the notations

$$k_0 = \omega/c, \tag{19a}$$

$$\epsilon(\vec{r}) = \begin{cases} 1 & \text{for } r<a, \\ \epsilon(\omega) & \text{for } r>a. \end{cases} \tag{19b}$$

The continuity of the fields and displacements at $r=a$ is guaranteed by the boundary conditions

$$[\epsilon(\omega)u]_{r=a^+} = (u)_{r=a^-}, \tag{20a}$$

$$\left(\frac{\partial}{\partial r}(ru)\right)_{r=a^+} = \left(\frac{\partial}{\partial r}(ru)\right)_{r=a^-}. \tag{20b}$$

The scalar field u has a singular part u^s associated with the direct-dipole field in vacuum. Its expression is obtained from Eq. (15) by using the expression of H_φ field of the direct dipole field:

$$u^s(r,\theta) = ip\frac{k_0}{r_0}\sum_l (2l+1)h_l^{(1)}(k_0 r_>) \times j_l(k_0 r_<)P_l(\cos\theta), \tag{21}$$

where p is the magnitude of the dipole moment, $h_l^{(1)}$ and j_l are spherical Hankel and Bessel functions, and $r_>$ ($r_<$) is the larger (smaller) of r and r_0.

The complete solution of Eq. (18) is

$$u(r,\theta) = u^s(r,\theta) + \sum_l A_l j_l(k_0 r)P_l(\cos\theta), \quad r<a, \tag{22a}$$

$$u(r,\theta) = \sum_l B_l h_l^{(1)}(k_1 r)P_l(\cos\theta), \quad r>a, \tag{22b}$$

where

$$k_1^2 = \epsilon(\omega)k_0^2.$$

The form (22a) is dictated by the fact that the singular part u^s has been extracted and reflected waves must remain everywhere finite, whereas the form (22b) expresses the outgoing-wave boundary condition at distances larger than a.

The unknown coefficients A_l and B_l are determined by Eqs. (20a) and (20b). The result is

$$A_l = (\alpha_l/M_l)\{h_l^{(1)}(z_0)[z_1 h_l^{(1)}(z_1)]' - \epsilon(\omega)h_l^{(1)}(z_1)[z_0 h_l^{(1)}(z_0)]'\}, \tag{23a}$$

$$B_l = (\alpha_l/M_l)\{h_l^{(1)}(z_0)[z_0 j_l(z_0)]' - j_l(z_0)[z_0 h_l^{(1)}(z_0)]'\}, \tag{23b}$$

where the prime means the first derivative, and

$$\alpha_l = ip(k_0/r_0)(2l+1)j_l(k_0 r_0), \tag{24a}$$

$$M_l = \epsilon(\omega)h_l^{(1)}(z_1)[z_0 j_l(z_0)]' - j_l(z_0)[z_1 h_l^{(1)}(z_1)]', \tag{24b}$$

with

$$z_i = k_i a \quad (i=0,1). \tag{25}$$

Note that the zeros of M_l give the eigenfrequencies of the void plasmons with the retardation included.[30] Hence there are resonances in the field amplitudes when the oscillator frequency coincides with one of the cavity eigenfrequencies. For the flat-metal surface geometry, such resonant cases have been discussed in Refs. 12–14.

Next one computes the radial component of the Poynting vector for $r<a$ by

$$S(r,\theta) = (c/4\pi)[\mathrm{Re}E_\theta(\vec{r})e^{i\omega t}][\mathrm{Re}H_\varphi(\vec{r})e^{i\omega t}].$$

After a somewhat lengthy calculation, one obtains for the total outward energy flow

$$S(r_0) \equiv \int S(r,\theta)r^2\sin\theta\,dr\,d\theta\,d\varphi = \frac{p^2}{4}k_0^3\omega\sum_l 2l(l+1)(2l+1) \times\left(\frac{j_l(k_0 r_0)}{k_0 r_0}\right)^2\left(1+\mathrm{Re}\frac{A_l}{\alpha_l}\right). \tag{26}$$

This expression gives the rate at which energy is lost by the oscillator. Hence the position-dependent energy-damping constant is

$$\gamma(r_0) = \gamma_0 + \frac{e^2k_0^3}{m\omega}\sum_l l(l+1)(2l+1) \times\left(\frac{j_l(k_0 r_0)}{k_0 r_0}\right)^2 \mathrm{Re}\frac{A_l}{\alpha_l}. \tag{27}$$

Here γ_0 is the isolated-dipole damping rate in vacuum as given by Eq. (2) [the proof that the first term of Eq. (26) gives rise to γ_0 in Eq. (27) is given in Appendix A]. The second term in Eq. (27) takes account of the surrounding metal and depends in a complicated manner on r_0 and a through Eqs. (23) and (24).

To see the Van der Waals shift due to the virtual

excitation of plasmons, we return to Eq. (16) and consider the equation of motion of the dipole moment. The electric field seen by the dipole is obtained from Eq. (16) and Eq. (22a) (ignoring the self-field u^s):

$$E_r(r=r_0,\theta=0) = \sum_l ipk_0^3\, l(l+1)(2l+1)\left(\frac{j_l(k_0r_0)}{k_0r_0}\right)^2 \frac{A_l}{\alpha_l}. \quad (28)$$

The equation of motion of the radial dipole oscillation is

$$\ddot{p}+\omega_0^2 p=(e^2/m)E_r(r=r_0,\theta=0), \quad (29)$$

where in our case $\hbar\omega_0=21.2$ eV. Thus the real part of Eq. (28) gives the Van der Waals shift, whereas the imaginary part reproduces the decay rate [the second term of Eq. (27)] as it should. Note that due to the factor l in Eq. (28) the monopole plasmon mode ($l=0$) does not contribute to the damping nor to the Van der Waals shift.

2. *Discussion of pure radiative effects*

To gain a qualitative understanding of the metal-substrate effect on the purely radiative width, let us consider the case where the dipole occupies the cavity center ($r_0=0$) and assume a real dielectric function ($g=0$) for the metal. The only surviving contribution to Eq. (27) comes from the dipole polariton $l=1$ [the contribution to Eq. (27) from real $\epsilon(\omega)$ is denoted as $\gamma_r(r_0)$]:

$$\gamma_r(0)/\gamma_0 = (1+\alpha\cos z_0-\beta\sin z_0)\Theta(\omega-\omega_0), \quad (30)$$

where $\Theta(x)=1$ for $x>0$ and $=0$ for $x<0$ and the two real constants α and β are defined by

$$\alpha+i\beta=\frac{(z_0+i)[z_1+(1-z_1^2)i]-\epsilon(\omega)(z_1+i)[z_0+(1-z_0^2)i]}{\epsilon(\omega)(z_1+i)[(z_0^2-1)\sin z_0+z_0\cos z_0]+[z_1+(1-z_1^2)i](\sin z_0-z_0\cos z_0)}. \quad (31)$$

The result (30) is plotted in Fig. 2 as a function of k_0a using the parameters of the He-Al system. One gets the following results; (i) When the oscillator frequency ω_0 is less than the metal-plasma frequency ω_p, the dipole field does not penetrate deeply into the metallic region because $\epsilon(\omega)<0$ for this frequency range. There is energy transfer back and forth between the atom and the cavity surface modes but this energy exchange goes on indefinitely if ϵ is assumed to be lossless. In other words, the light gets indefinitely reflected by the concave metal surface and the energy remains

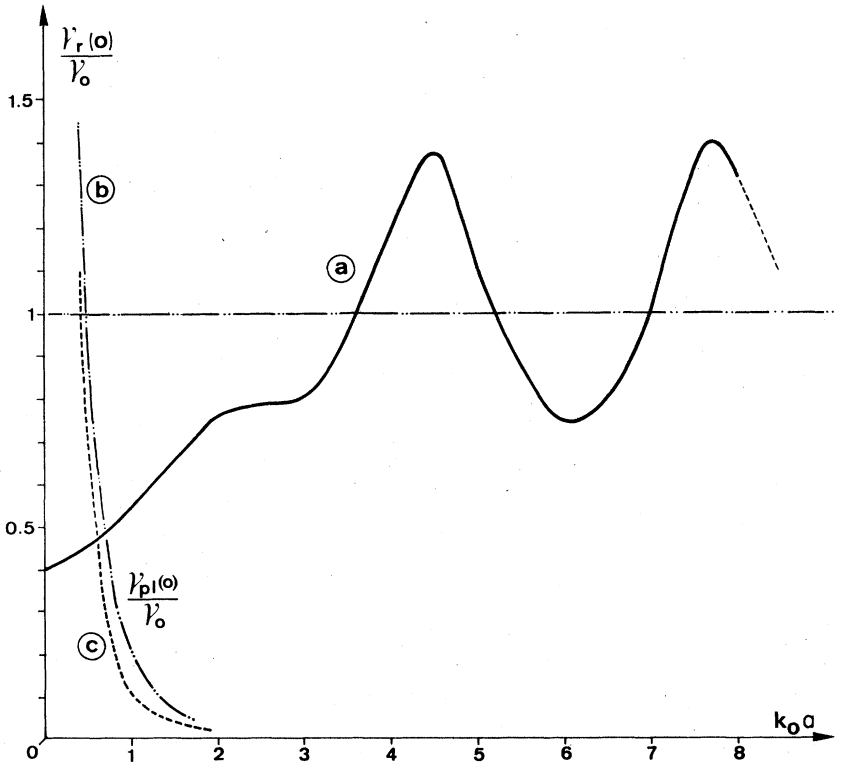

FIG. 2. (a) Oscillatory radiation linewidth for an atom at the center of a spherical cavity in a metal of real dielectric function, as a function of reduced cavity radius ($k_0a=1$ for $a\simeq 90$ Å in the He case); (b) and (c): nonradiative width obtained when including surface plasmon damping with two values of the damping constant: $g=4$ eV (b) and $g=2$ eV (c).

confined within a few radii around the cavity. This conclusion also holds true for any position of the atom in the cavity. This is in clear contrast to the case of a flat-metal surface.[12-14] For the planar geometry, energy can effectively be drained away at an infinite distance either towards the semi-infinite free space or along any direction within the planar surface even though, ϵ being real and negative, energy cannot be radiated towards the interior of the metallic half space. Mathematically, the fact that $\gamma_r/\gamma_0=0$ when $\omega<\omega_p$ is implicit in Eqs. (30) and (31). Indeed when $\epsilon<0$, z_1 is purely imaginary and a simple algebraic calculation then shows that $1+\alpha\cos z_0-\beta\sin z_0\equiv 0$ so that the Θ step function in Eq. (30) is simply redundant.

(ii) From Fig. 2 one sees that for $\omega>\omega_p$ and in the limit $a\to 0$, the damping rate approaches a finite value:

$$\lim_{a\to 0}\frac{\gamma_r(0)}{\gamma_0}=\frac{9\epsilon(\omega)^{3/2}}{[1+2\epsilon(\omega)]^2}. \tag{32}$$

Apart from the factor $9/[1+2\epsilon(\omega)]^2\simeq 2.2$, $\gamma_r(0)$ is equal to γ_0 as given by Eq. (2) in which k_0 is replaced by $\sqrt{\epsilon}k_0$, the wave vector of the radiation in the metallic region. The dipole lifetime is somewhat increased due to multiple reflection and reexcitation effects. Note that the apparent resonance of the denominator at $\epsilon(\omega)=-\frac{1}{2}[\omega=\omega_p(\frac{2}{3})^{1/2}]$ is not real since $\gamma_r(0)=0$ for $\omega<\omega_p$ as discussed in (i).

(iii) For real $\epsilon(\omega)$, the effect of the metal substrate does not vanish in the limit of very large bubble radius. Indeed $\gamma_r(0)$ is seen to oscillate with the periodicity $k_0a=\pi$. The asymptotic formula is, from Eqs. (30) and (31),

$$\lim_{a\to\infty}\frac{\gamma_r(0)}{\gamma_0}=\frac{[\epsilon(\omega)]^{1/2}}{\epsilon(\omega)\sin^2 z_0+\cos^2 z_0}. \tag{33}$$

Thus $\gamma_r(0)$ oscillates between the extreme values $\gamma_0\epsilon^{-1/2}$ and $\gamma_0\epsilon^{1/2}$. Such oscillatory behavior is easily understood as due to a phase-matching effect between the oscillator amplitude and the reflected wave which has traveled twice the cavity radius. Note that in the flat-metal surface case, the effect of the surface decays as z^{-2} in the limit $z\to\infty$ (z is the distance between the dipole and the metal surface), as is shown by extending the calculation of Ref. 12, for example.

(iv) When $\epsilon(\omega)$ is real, the damping width $\gamma_r(0)$ is of the same order of magnitude as γ_0, irrespective of the cavity radius.

3. *Inhomogeneous line shift and width*

Since we are interested in large enhancements of linewidth over the natural width γ_0, we see from the general result (28) that we should work in the limit where $k_0a<1$, i.e., small bubble radii as compared to the vacuum wavelength of 584.3 Å (in fact, one should have $a<k_0^{-1}\simeq 90$ Å). For such small radii, we are justified to neglect retardation effects altogether by assuming $c\to\infty$ in formula (28).

Taking the limit $c\to\infty$ of Eq. (27) or Eq. (28) is easily done by returning to Eqs. (23) and (24). From Eq. (29) one obtains

$$\omega^2-\omega_0^2=\omega_0^2\frac{\alpha_0}{a^3}\times\sum_l l(l+1)\left(\frac{r_0}{a}\right)^{2(l-1)}\frac{1-\epsilon(\omega)}{1+[(l+1)/l]\epsilon(\omega)}, \tag{34}$$

where

$$\alpha_0=e^2/m\omega_0^2$$

is a measure of the He ground-state polarizability. The right-hand side of Eq. (34) has a resonance at the frequency determined by

$$l+(l+1)\epsilon(\omega)=0 \text{ or } \omega=\omega_l\equiv\left(\frac{l+1}{2l+1}\right)^{1/2}\omega_p, \tag{35}$$

i.e., at the frequency of the cavity surface plasmon of angular momentum (l,m).[30] If the dipole frequency ω coincides with one of these plasmon frequencies, the corresponding term in Eq. (34) may get quite large and Eq. (34) should be solved nonperturbationally by using, say, Eq. (B7) in Appendix B. For our He-Al system, however, one is far from resonance so that we may safely put ω equal to ω_0 in the right-hand side of Eq. (34).

To compare the decay rate due to the plasmon excitation with the radiation damping, we plotted in Fig. 2 the energy-damping constant for the center position $r_0=0$. We see that for reasonable values of g the plasmon-damping effect dominates the radiative damping for small voids (i.e., $k_0a<1$), as was mentioned before.

The summation over l in Eq. (34) is performed in Appendix B and in Fig. 3 we plot the energy-damping constant $\gamma_{pl}(r_0)$ as a function of the distance z from the void wall ($z=a-r_0$) for three values of the void radius $a=5$, 10 Å, and $a=\infty$. The last case corresponds to the flat-metal surface:

$$\omega^2-\omega_0^2=\omega_0^2\frac{2\alpha_0}{(2z)^3}\frac{1-\epsilon(\omega)}{1+\epsilon(\omega)}. \tag{36}$$

From the figure we see the following.

(a) The finiteness of the curvature manifests itself mostly when the dipole is near the center of the cavity. Just at $r_0=0$, the only contribution comes from the $l=1$ mode as before.

(b) For $r_0\simeq a$ or $z\simeq 0$, the damping constant becomes enhanced and diverges at $z=0$. It is interesting to note that this r_0 dependence comes from the multipolar modes of order higher than $l=1$,

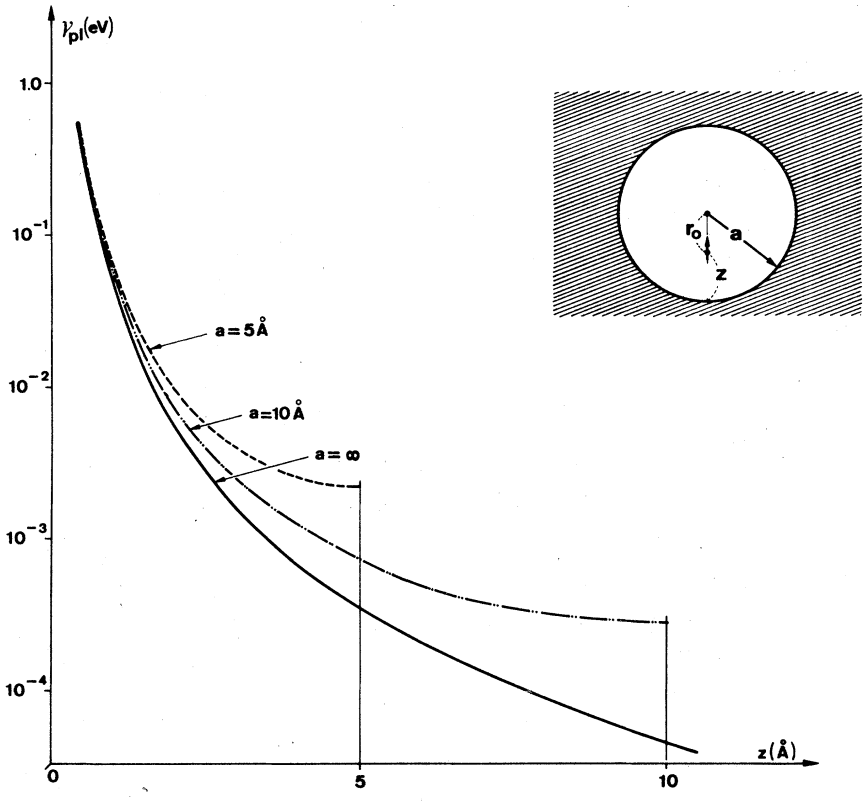

FIG. 3. Linewidth due to atom-plasmon coupling as a function of atom distance from the wall surface and for several cavity radii.

since the contribution from $l=1$ is r_0 independent. When $z \to 0$, the summation in Eq. (34) should be truncated at some maximum value of l determined by the void radius, according to $l \leq k_c a$, where k_c is the plasmon cutoff wave vector.[11] This effect removes the divergence at $z=0$. However, an actual calculation which incorporates the cutoff shows that this effect is appreciable only for $z \leq 2$ Å, as shown in Fig. 4.

(c) For z less than 3 Å Eq. (34) is practically the same as the flat surface formula (36).

For the frequency shift [real part of Eq. (34)], analogous discussions can be performed. In the following discussion of the line shapes we shall use an approximate formula obtained as follows. Let us replace the factor $(l+1)/l$ in the denominator of Eq. (34) by some constant λ $(1 \leq \lambda \leq 2)$ independent of l. This procedure corresponds to replacing the l-dependent frequency ω_l [Eq. (35)] by some average cavity-plasmon frequency. Then the remaining l summation of Eq. (34) is a simple geometrical series. We get the simple analytical expression:

$$\omega^2 - \omega_0^2 = \frac{2\omega_0^2 \alpha_0}{a^3} \frac{a^6}{(a^2 - r_0^2)^3} \frac{1-\epsilon(\omega)}{1+\lambda\epsilon(\omega)} . \qquad (37)$$

This formula correctly predicts the actual shift and decay rate in the two extreme cases

$$\lim_{r_0 \to 0} (\omega^2 - \omega_0^2) = \frac{2\omega_0^2 \alpha_0}{a^3} \frac{1-\epsilon(\omega)}{1+2\epsilon(\omega)} \quad (\lambda = 2) \qquad (38)$$

for the atom at the center of the cavity and

$$\lim_{r_0 \to a} (\omega^2 - \omega_0^2) = \frac{2\omega_0^2 \alpha_0}{(2z)^3} \frac{1-\epsilon(\omega)}{1+\epsilon(\omega)} \quad (\lambda = 1) \qquad (39)$$

for the flat-metal-surface situation. Since the excitation frequency of the He is well separated from the narrow range $\omega_p/\sqrt{2} < \omega_l < \omega_p \sqrt{\frac{2}{3}}$ and since an actual r_0 dependence of the local density $n(r_0)$ involved in Eq. (14) is not at hand, the approximate formula (37) is certainly sufficient for the discussion of the line shapes.

Let us return to Eq. (14) and first calculate the line shape arising from the inhomogeneous line shift alone. Assuming zero damping [real $\epsilon(\omega)$] and a uniform density n, Eq. (14) reduces to

$$I(\omega) = n \int_0^{a-z_0} r_0^2 \delta(\omega - \omega(r_0)) dr_0$$

$$= n r_0(\omega)^2 \frac{dr_0(\omega)}{d\omega} , \qquad (40)$$

where from Eq. (37) the position-dependent oscillator frequency is

$$\omega^2(x) = \omega_0^2 [1 + \kappa/(1-x)^3] , \qquad (41)$$

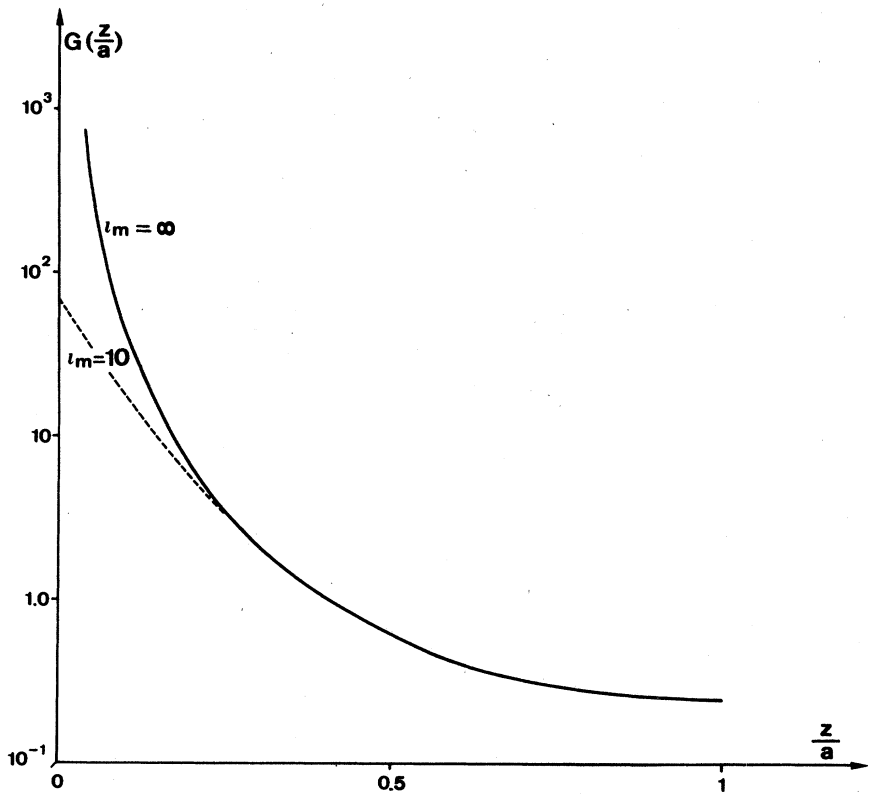

FIG. 4. Effect of finite-cutoff angular momentum l_m of the plasmons on the plasmon-related width written as $\gamma_{pl}/\gamma_0 = (k_0 a)^{-3} G(z/a)$. One sees that the finite cutoff removes the z^{-3} divergence due to higher angular momenta.

with

$$x = (r_0/a)^2,$$
$$\kappa = \frac{2\alpha_0}{a^3}\frac{1-\epsilon(\omega_0)}{1+\lambda\epsilon(\omega_0)}, \tag{42}$$

and $r_0(\omega)$ in Eq. (40) is implicitly given by Eq. (41). Letting

$$y = \omega/\omega_0,$$
$$u = (y^2-1)/\kappa \simeq 2(y-1)/\kappa, \tag{43}$$

one obtains the universal line shape

$$I(y) = n\sqrt{x}(1-x)^4$$
$$= n(1-u^{-1/3})^{1/2}u^{4/3}. \tag{44}$$

This is plotted in Fig. 5 for a void of radius $a = 10$ Å, taking $\alpha = 0.15$ Å^3 for the He polarizability and $\lambda = \frac{3}{2}$ ($\kappa \simeq 10^{-4}$). The line shape is seen to be highly asymmetrical with a maximum (at $r_0 = \frac{1}{3}a$, $x = \frac{1}{9}$, $u \simeq 1.4$) very close to ω_0 and a long tail towards higher frequencies. The linewidth is roughly $\Delta u \simeq 4$, i.e.,

$$\Delta\omega/\omega_0 \simeq 2\kappa \simeq 2\times 10^{-4} \tag{45}$$

for the example considered.

One sees that the broadening due to inhomogeneous Van der Waals shift is indeed quite small for cavities of radii larger than, say, 10 Å.

For smaller voids and ultimately for substitutional He in a single atomic vacancy, one may attempt to extrapolate the above results. Taking $a = 2$ Å for Al as the size of the vacancy and assuming single He occupation at the vacancy center, Eq. (38) predicts a maximum shift of

$$(\omega-\omega_0)/\omega_0 \simeq 0.01. \tag{46}$$

Only if a substantial fraction of implanted He remains in substitutional sites or very small vacancy clusters may this shift manifest itself in the absorption spectrum both as a shift and as a broadening. However one should recall that for He trapped in vacancies (even more than for physisorbed He) the mechanism discussed earlier of electron hopping from the He $2P$ excited state into the metal conduction-band states is expected to provide another important source of line shift and width, perhaps more important than Eq. (46).

One can analyze, in a similar fashion, the broadening due to the imaginary part of Eq. (37) assuming a complex dielectric function as in Eq. (13) with some reasonable g value.

From Eqs. (14) and (37) the full line shape which combines both inhomogeneous shift and width due

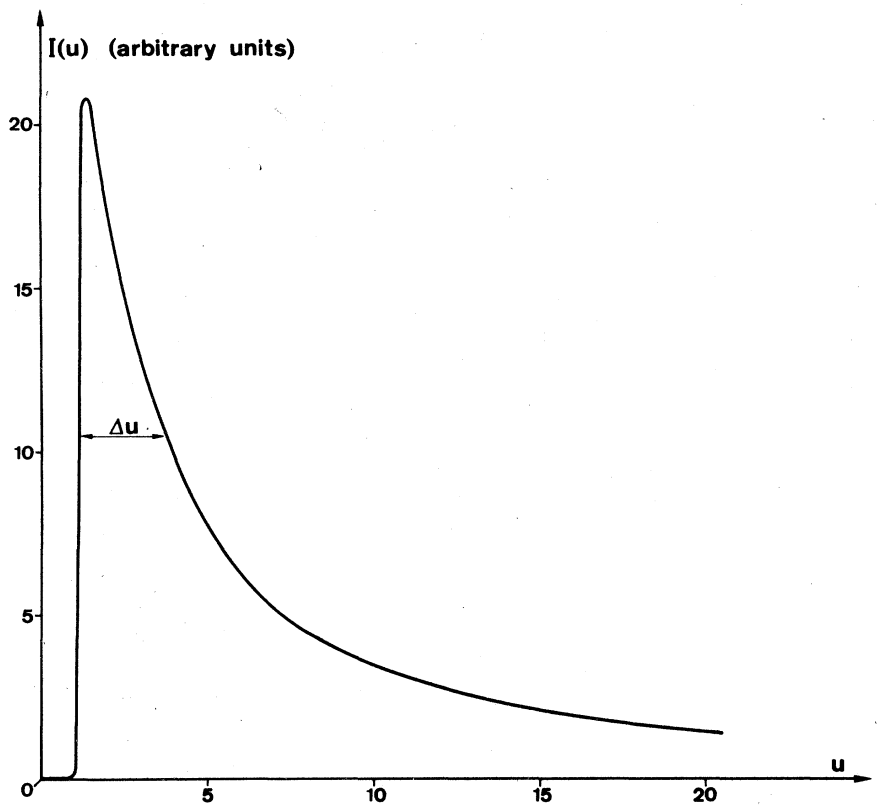

FIG. 5. Universal line shape of Eq. (44) (see text) illustrating the broadening due to inhomogeneous Van der Waals of the atomic line.

to plasmons is

$$I(y) = n \operatorname{Im} \int_0^{1-\zeta} dx \, \frac{x^2}{y - 1 - \beta(1-x^2)^{-3}} , \qquad (47)$$

where $y = \omega/\omega_0$ as before and

$$\zeta = z_0/a ,$$

$$\beta = \beta_R + i\beta_I = \frac{\alpha_0}{a^3} \frac{1-\epsilon(\omega)}{1+\lambda\epsilon(\omega)} \simeq \frac{\alpha_0}{a^3} \frac{1}{25}(7+2i) , \qquad (48)$$

the last equality being obtained by taking $g \simeq 4$ eV in Eq. (13). Equation (47) can be written

$$I(y) = n \operatorname{Im} \frac{\beta}{y-1} \int_0^{1-\zeta} dx \, \frac{x^2}{(y-1)(1-x^2)^3 - \beta} . \qquad (49)$$

The integral can be obtained analytically (rational function) but the result is too lengthy to report here. Figure 6 shows the resulting line shape for typical values of the parameters. Again it is seen to be highly asymmetrical and relatively narrow for bubbles of not too small radii. The width is of order $\Delta y = \Delta\omega/\omega_0 \simeq 2.8 \times 10^{-4}$, slightly larger than the inhomogeneous shift Eq. (45).

IV. BUBBLE ABSORPTION FROM EFFECTIVE-MEDIUM THEORY

The results of Sec. III for the bubble-absorption line shape were obtained by statistically averaging the absorption spectrum of single independent atoms in the metal cavity. However for all bubbles whose size is smaller than the wavelength, all atoms in it absorb coherently in an electric field essentially uniform over the bubble diameter. This effect may be taken into account by using a different approach in which the gas bubbles are viewed as macroscopic spherical inclusions of homogeneous dielectric function $\epsilon_g(\omega)$ randomly and homogeneously dispersed in the metal matrix. The system is complementary to small solid particles dispersed in a gas and, when the sphere radii are smaller than the wavelengths of interest, the optical properties of the composite medium may be formulated in terms of an effective-medium approach.

A detailed discussion of the available effective-medium theories has recently been given by Grandqvist and Hunderi.[17] All theories eventually coincide when the so-called "filling" factor f (i.e., the volume fraction occupied by the spheres, which

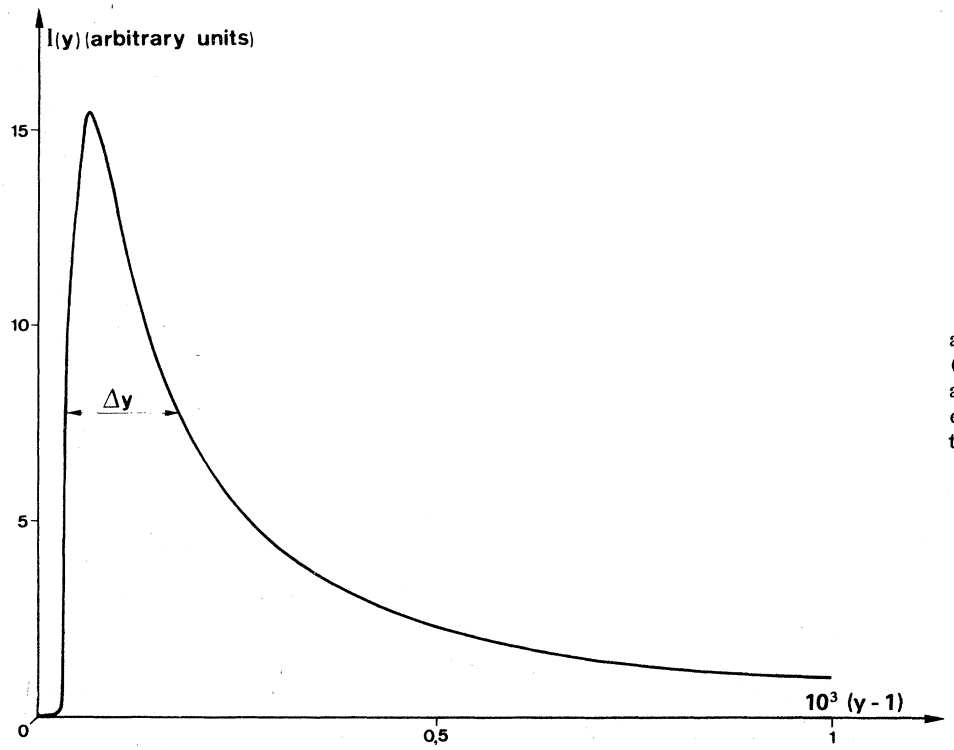

FIG. 6. Line shape of the atomic line as given by Eq. (49) in the text and taking account of both inhomogeneous shift and damping due to plasmons.

in our context is in effect an "unfilling" factor and will be, more appropriately, called the swelling factor) is sufficiently small, say less than 10%. In this small swelling limit, the optical properties may be obtained from an average dielectric function $\bar{\epsilon}$ given by[15-17]

$$\bar{\epsilon} = \epsilon + 3f\epsilon(\epsilon_g - \epsilon)/(\epsilon_g + 2\epsilon), \tag{50}$$

valid up to first order in f.

For the metal dielectric function $\epsilon(\omega)$, we keep using expression (13) whereas for the gas $\epsilon_g(\omega)$ we are led to use the Clausius-Mossotti form

$$\epsilon_g(\omega) = 1 + 4\pi n\alpha(\omega)/[1 - \tfrac{1}{3}4\pi n\alpha(\omega)], \tag{51}$$

in which n is the gas density and $\alpha(\omega)$ is the gas-atom dynamical polarizability.

It will be recalled that this basic formula for ϵ_g includes the dipole interactions between the gas atoms when the external field which they experience is uniform over the occupied region of space. The local field is changed by the Lorentz field of the uniform distribution of dipoles. For the polarizability $\alpha(\omega)$ we take a single oscillator, Drude form

$$\alpha(\omega) = \alpha_0\,\omega_0^2/[\omega_0^2 - \omega(\omega + i\gamma_g)], \tag{52}$$

where α_0 is, as before, the static atomic polarizability and where γ_g is the linewidth. Since $\epsilon_g(\omega)$ should correctly describe the properties of the pure gas in its actual pressure state within the bubbles, we are led to identify γ_g with the resonance broadening width discussed in Sec. II C. Here we shall use[21]

$$\gamma_g/\omega_0 = 2\pi n\alpha_0, \tag{53}$$

assuming that all bubbles have a common gas density n. This rather strong assumption restricts the validity of the present treatment to the fairly frequent case of narrow bubble-size distribution. It can be lifted in a more quantitative theory if an actual size—and hence density—histogram is taken into account.[17]

The pole of $\epsilon_g(\omega)$ occurs at the frequency

$$\omega = \omega_0(1 - \tfrac{1}{3}2\pi n\alpha_0), \tag{54}$$

slightly red shifted with respect to the atomic line position ω_0 due to the dipole interactions. The absorption Lorentzian $\mathrm{Im}\epsilon_g(\omega)$ appropriate to the He gas alone is plotted as the dashed curve in Fig. 7. The width of this line is given in (53).

The composite-medium dielectric function $\bar{\epsilon}(\omega)$, on the other hand, is seen, from (50), to have poles at

$$\epsilon_g(\omega) + 2\epsilon(\omega) = 0, \tag{55}$$

i.e., if the damping terms γ_g and g are neglected, at

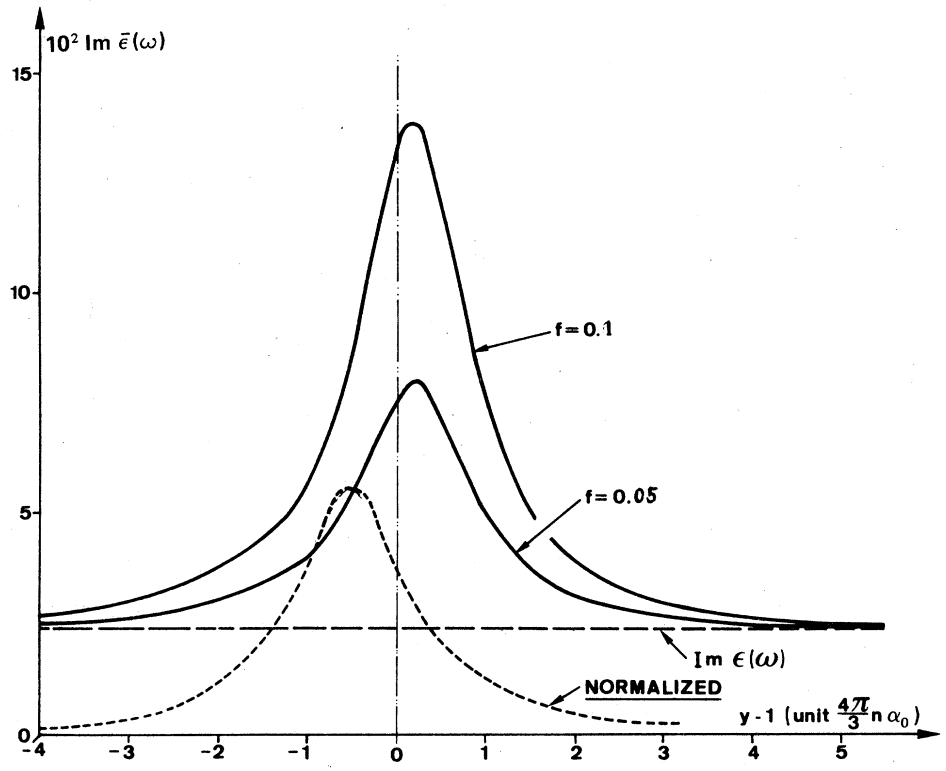

FIG. 7. Absorption line shape Im $\bar{\epsilon}$ (ω) of the He-Al system around the free-atom resonance line ω_0 [Eq. (50)]. The dotted Lorentzian is the infinite gas absorption at density n. The full Lorentzians give the absorption of He spherical bubbles, above the Al-metal background shown as Im ϵ (ω), for two values of the swelling factor f. The dotted line is arbitrarily normalized to the same heights as the $f=0.05$ line.

$$\omega = \sqrt{\tfrac{2}{3}}\,\omega_p\left[1 - \tfrac{1}{2}\,4\pi n\alpha_0\,\omega_p^2/(3\omega_0^2 - 2\omega_p^2)\right], \qquad (56)$$

and

$$\omega = \omega_0\left[1 + \tfrac{1}{3}\,4\pi n\alpha_0\,\omega_p^2/(3\omega_0^2 - 2\omega_p^2)\right]. \qquad (57)$$

One obtains two Lorentzian absorption peaks in Im$\bar{\epsilon}(\omega)$, one centered around (56) with width of order g and one around (57) of width γ_g. The first line gives the absorption of the dipole plasmon of the bubble slightly red shifted by the presence of the trapped gas and the second line is the gas absorption, blue shifted by the metal substrate. This atomic line is illustrated in Fig. 7 for the He-Al case for two values of the swelling factor f to which the absorption strength is roughly proportional.

The above results are correct up to first order in $4\pi n\alpha_0$ and off resonance. If the resonance condition $3\omega_0^2 - 2\omega_p^2 \simeq 0$ is satisfied, the correct solutions of (55) are

$$\omega_\pm = \frac{\omega_0}{\sqrt{6}}\left\{3 + 2\,\frac{\omega_p^2}{\omega_0^2} \pm \left[\left(3 - 2\,\frac{\omega_p^2}{\omega_0^2}\right)^2 + 32\pi n\alpha_0\,\frac{\omega_p^2}{\omega_0^2}\right]^{1/2}\right\}^{1/2}, \qquad (58)$$

and Im$\bar{\epsilon}$ has peculiar behavior which we shall not investigate here.

V. CONCLUSIONS

The aim of the present work was to examine a number of broadening mechanisms for an optical transition line of an atom trapped in a metal cavity and to estimate the absorption spectrum of gas bubbles. Particularly the line shape resulting from long-range multipole interaction with the surface polaritons of the substrate was studied in detail.

If the dielectric function $\epsilon(\omega)$ of the substrate can be treated as real, two major effects associated with the substrate occur: (i) The linewidth vanishes when the line frequency ω renders $\epsilon(\omega)$ negative. In the free-electron model, this occurs when ω is less than the plasma frequency ω_p; (ii) The linewidth is oscillatory as a function of cavity radius for frequencies higher than ω_p and never tends to the free-space natural linewidth, irrespective of cavity radius.

Both effects result from reflections and interferences of emitted photons by the concave cavity surface and are in clear contrast to the effects occurring with flat surfaces. These conclusions show that it is important in curved geometries to take account of the imaginary part of $\epsilon(\omega)$ which

brings about polariton damping and, hence, enhanced atomic excitation damping.

We have formulated the problem in full generality, within the classical framework of Maxwell's equations, and obtained an exact expression [Eq. (27)] for the overall polariton linewidth.

In applying the theory to an example of practical interest, namely, the resonance line of He trapped in bubbles in Al, we have neglected retardation effects in view of the fact that in many instances the bubbles have radii smaller than the vacuum wavelength (584 Å) of the He radiation. Then the shift and shape of the atomic line is governed by Van der Waals interactions with the substrate through the nonretarded damped-surface plasmons of the cavity. The new result [Eq. (38)] also applies to the limiting case of infinite cavity radius, i.e., to an atom near a flat-metal surface, and agrees with previous results obtained by other authors for this situation.[12-14] The theory predicts large shifts and broadening of the line when its frequency happens to coincide with one of the cavity plasmon frequencies.

In the He-Al system, because of the smallness of the He polarizability and of the fact that the He resonance line frequency is substantially larger than the plasmon frequencies, the plasmon-induced width, amounting to $\gamma_{\rm pl}/\omega_0 \simeq$ (a few times) α_0/a^3, remains rather modest except of course for cavities of radii smaller than, say, 10 Å. Similar conclusions are obtained by an analysis of the optical properties of the porous metal in terms of an effective-medium dielectric constant, along the lines of the old Maxwell-Garnet theory[32] for multiphase media. This approach leads to both shift and width of the He excitation proportional to the assumed common density in the bubbles (a distribution of different densities in variable-size bubbles may also be treated). This result is rather favorable if one is to use the resonant absorption line shape of He to obtain an indirect measure of the gas pressure in the bubbles, as proposed in the Introduction.[19]

ACKNOWLEDGMENTS

This work was performed under auspices of the IRIS project (Institute for Research in Interface Sciences) sponsored by the Belgian Ministry for Science Policy.

The authors are indebted to their colleagues, Professors J. M. Gilles, R. Caudano, L. Laude, R. Dagonnier and W. McGowan for helpful discussions on the subject of this paper. One of us (K.O.) acknowledges the financial support of the Administration of Belgo-Japanese Cultural Agreements and the Facultés Universitaires N.D. de la Paix. One of us (A.A.L.) is grateful to the NATO Scientific Affairs Division for partial support of this work.

APPENDIX A

To prove that the first term of Eq. (26) gives rise to γ_0 in Eq. (27), we establish the identity

$$F(z)=\sum_{l=1}^{\infty} l(l+1)(2l+1)\left(\frac{j_l(z)}{z}\right)^2=\frac{2}{3}\,. \tag{A1}$$

Differentiate (A1)

$$\frac{dF(z)}{dz}=2\sum_l l(l+1)(2l+1)\frac{j_l}{z}\left(\frac{j_l'}{z}-\frac{j_l}{z^2}\right)$$
$$\equiv g_1(z)-g_2(z)\,. \tag{A2}$$

Eliminate j_l' in $g_1(z)$ by using the identity[31]

$$(2l+1)j_l'=l j_{l-1}-(l+1)j_{l+1}\,. \tag{A3}$$

We get

$$g_1(z)=\frac{2}{z^2}\sum_l 2(l+1)^2 j_l j_{l+1}\,. \tag{A4}$$

On the other hand, use of the recurrence formula[31]

$$(2l+1)j_l/z=j_{l+1}+j_{l-1}\,, \tag{A5}$$

in $g_2(z)$ leads to $g_2(z)=g_1(z)$ and hence $F'(z)=0$ or $F(z)=$ const whose value is obtained by taking the limit $z=0$ in (A1), remembering that $\lim_{z\to 0} j_l(z)/z = \frac{1}{3}\delta_{l,1}$.

APPENDIX B

To obtain the analytic form of Eq. (34), let us write the right-hand side of Eq. (34) as

$$\omega_0^2\frac{\alpha_0}{a^3}\left(\frac{r_0}{a}\right)^{-2}\frac{1-\epsilon(\omega)}{1+\epsilon(\omega)}F(u,v)\,, \tag{B1}$$

with

$$F(u,v)=\sum_{l=1}^{\infty}\frac{l^2(l+1)}{l+u}v^l\,, \tag{B2}$$

where

$$u=\epsilon(\omega)/[1+\epsilon(\omega)]\,, \tag{B3a}$$

$$v=(r_0/a)^2\,. \tag{B3b}$$

The decomposition of Eq. (B2) leads to

$$F(u,v)=\sum_l\left(l^2v^l+(1-u)lv^l-u(1-u)v^l\right.$$
$$\left.+u^2(1-u)\frac{v^l}{l+u}\right). \tag{B4}$$

The first three series of Eq. (B4) are easily obtained (note that $0<v<1$). The fourth series is obtained by help of the relation

$$\sum_{l=1}^{\infty}\frac{v^l}{l+u}=v\int_0^1\frac{t^u}{1-vt}dt\,. \tag{B5}$$

Equation (B5) is valid[31] for $\mathrm{Re}\,u>-1$, i.e., ω

$>(\frac{2}{3})^{1/2}\omega_p$ in the case of real $\epsilon(\omega)$. The expression valid for any complex value of u is derived by the analytical continuation of Eq. (B5). The result is

$$\sum_{l=1}^{\infty}\frac{v^l}{l+u}=\frac{e^{-i\pi u}}{2i\sin\pi u}v\int_C\frac{t^u}{1-vt}dt\,, \tag{B6}$$

where the contour C in the complex t plane is shown in Fig. 8. Equation (B6) has resonances at $u=-1,-2,-3,\ldots$, i.e., at $\omega=\omega_l$ [Eq. (35)] and provides a convenient expression for analyzing the resonant case where ω lies in the region $(\frac{1}{2})^{1/2}\omega_p<\omega<(\frac{2}{3})^{1/2}\omega_p$.

From Eqs. (B4) and (B7) one obtains

$$F(u,v)=\frac{v(1+v)}{(1-v)^3}+(1-u)\frac{v}{(1-v)^2}-u(1-u)\frac{v}{1-v}$$

$$+u^2(1-u)\,[\text{Eq. (B6)}]\,. \tag{B7}$$

To obtain the expression for the flat-metal case we have only to put $r_0=a-z$ and take the limit $a\to\infty$ with constant z. Due to the a^{-3} factor in Eq. (B1), the only remaining contribution to Eq. (34) occurs from the first term of Eq. (B7), from which follows Eq. (36) in the text.

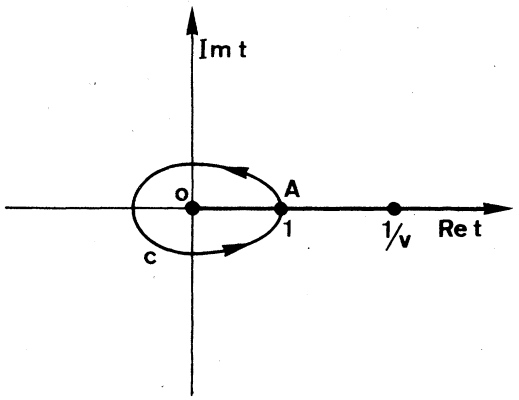

FIG. 8. Integration contour C in the complex t plane for Eq. (B6.). The argument of the departure point A is taken such that t^u is real.

*On leave from Dept. of Applied Physics, Faculty of Engineering, The University of Tokyo, Bunkyo-ku, 113 Tokyo, Japan.

[1]D. J. Mazey, B. L. Eyre, J. H. Evans, S. K. Erents, and G. M. McCracken, J. Nucl. Mater. 64, 145 (1977).
[2]F. A. Smidt and A. G. Pieper, *Properties of Reactor Structural Alloys or Particle Irradiation*, ASTM No. STP 570 (American Society for Testing and Material, Philadelphia, Penn., 1975).
[3]*Applications of Ion Beams to Metals*, edited by S. T. Picraux, E. P. Eernisse, and F. L. Vook (Plenum, New York, 1974).
[4]*Radiation-Induced Voids in Metals*, edited by J. W. Corbett and L. C. Ianniello, (SAEC, Oak Ridge, 1972).
[5]International Conference on Radiation Effects and Tritium Technology for Fusion Reactors, ERDA Conf. No. 750989, 1975 (unpublished).
[6]R. Bullough and R. C. Perrin, *Radiation on Damage in Reactor Materials* (IAEA, Vienna, 1969), Vol. II, p. 233.
[7]J. H. Evans, J. Nucl. Mater. 68, 129 (1977).
[8]J. R. Cost and K. Y. Chen, J. Nucl. Mater. 67, 265 (1977).
[9]G. Herzberg, *Atomic Spectra and Atomic Structure*, 2nd ed. (Dover, New York, 1944).
[10]P. Lee and G. L. Weissler, Phys. Rev. 99, 540 (1955).
[11]D. Pines, *Elementary Excitations in Solids* (Benjamin, New York, 1964).
[12]H. Morawitz and M. R. Philpott, Phys. Rev. 10, 4863 (1974).
[13]R. R. Chance, A. Prock, and R. Silbey, Phys. Rev. A 12, 1448 (1975).
[14]G. S. Agarwal and H. D. Vollmer, Phys. Status Solidi B 79, 249 (1977), and references therein to previous work.
[15]A. S. Barker, Jr., Phys. Rev. 7, 2507 (1973).
[16]L. Genzel and T. P. Martin, Surf. Sci. 34, 33 (1973).
[17]C. G. Granqvist and O. Hunderi, Phys. Rev. 16, 3513 (1977).
[18]M. Born and E. Wolf, *Principle of Optics* (Pergamon, New York, 1964), p. 633.
[19]Measurements are under way at our laboratory, in conjunction with the DESY Synchrotron Radiation Laboratory in Hambourg.
[20]H. Margenau and W. W. Watson, Rev. Mod. Phys. 8, 22 (1936).
[21]R. G. Breene, *The Shift and Shape of Spectral Lines* (Pergamon, New York, 1961).
[22]B. Schiff and C. L. Pekeris, Phys. Rev. 134, A638 (1964).
[23]R. P. McEachran, A. G. Ryman, and A. D. Stauffer, J. Phys. B 10, L681 (1977).
[24]J. H. Evans, J. Nucl. Mater. 68, 129 (1977).
[25]H. G. Kuhn and J. M. Vaughn, Proc. R. Soc. A 277, 297, (1964).
[26]J. O. Hirshfelder, Ch. F. Curtis, and K. B. Bird, *Molecular Theory of Gases and Liquids* (Wiley, New York, 1954).
[27]J. E. Cunningham *et al.*, J. Phys. F 7, L281 (1977).
[28]H. J. Hagemann, W. Gudat, and C. Kunz, J. Opt. Soc. Am. 65, 742 (1975); and DESY Report No. SR-74/7, 1974 (unpublished).
[29]A. Sommerfeld, *Partial Differential Equation in Physics* (Academic, New York, 1949), p. 236.
[30]See, e.g., R. Engleman and R. Ruppin, Rep. Prog. Phys. 33, 149 (1970).
[31]M. Abramowitz and I. A. Stegun, *Handbook of Mathematical Functions* (Dover, New York, 1964), p. 437.
[32]J. C. Maxwell-Garnet, Philos. Trans. R. Soc. 203, 385 (1904); 205, 237 (1906).